Research article JHEP|Reports

Downregulation of 15-PGDH enhances MASH-HCC development via fatty acid-induced T-cell exhaustion

Authors

Xichen Hu, Tadahito Yasuda, Noriko Yasuda-Yosihara, Atsuko Yonemura, Terumasa Umemoto, Yutaka Nakachi, Kohei Yamashita, Takashi Semba, Kota Arima, Tomoyuki Uchihara, Akiho Nishimura, Luke Bu, Lingfeng Fu, Feng Wei, Jun Zhang, Yilin Tong, Huaitao Wang, Kazuya Iwamoto, Takaichi Fukuda, Hayato Nakagawa, Koji Taniguchi, Yuji Miyamoto, Hideo Baba, Takatsugu Ishimoto

Correspondence

taka1516@kumamoto-u.ac.jp (T. Ishimoto), kumasyuwa@gmail.com (T. Yasuda).

Graphical abstract

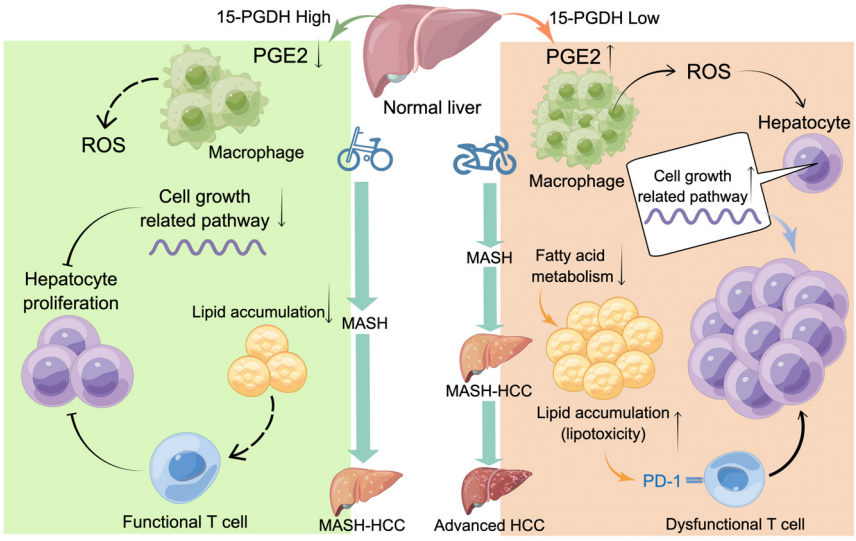

Highlights

- 15-*PGDH* downregulation in the background liver is correlated with the occurrence of MASH-HCC.
- The accumulation of PGE2 mediated by 15-*Pgdh* downregulation promotes hepatocyte proliferation.
- 15-*Pgdh* downregulation in murine hepatocytes promotes lipid accumulation in the TME.
- Lipid accumulation in the TME reduces mitochondrial activity and causes CD8+ T-cell exhaustion.

Impact and implications

The suppression of PGE2-related inflammation and subsequent lipid accumulation leads to a reduction in the severity of MASH and inhibition of subsequent progression toward MASH-HCC.

https://doi.org/10.1016/j.jhepr.2023.100892

Research article

JHEP|Reports

Downregulation of 15-PGDH enhances MASH-HCC development via fatty acid-induced T-cell exhaustion

Xichen Hu,[1,2] Tadahito Yasuda,[1,2,*] Noriko Yasuda-Yosihara,[1,2] Atsuko Yonemura,[1,2,3] Terumasa Umemoto,[4] Yutaka Nakachi,[5] Kohei Yamashita,[1,2] Takashi Semba,[1,3] Kota Arima,[2] Tomoyuki Uchihara,[1,2] Akiho Nishimura,[1,3,6] Luke Bu,[1,2] Lingfeng Fu,[1,2,3] Feng Wei,[1,2] Jun Zhang,[1,2] Yilin Tong,[1,2,3] Huaitao Wang,[1,2,3] Kazuya Iwamoto,[5] Takaichi Fukuda,[7] Hayato Nakagawa,[8] Koji Taniguchi,[9] Yuji Miyamoto,[2] Hideo Baba,[2,10] Takatsugu Ishimoto[1,2,3,*]

[1]*Gastrointestinal Cancer Biology, International Research Center for Medical Sciences (IRCMS), Kumamoto University, Kumamoto, Japan;* [2]*Department of Gastroenterological Surgery, Graduate School of Medical Sciences, Kumamoto University, Kumamoto, Japan;* [3]*Division of Carcinogenesis, The Cancer Institute, Japanese Foundation for Cancer Research, Tokyo, Japan;* [4]*Hematopoietic Stem Cell Engineering, International Research Center of Medical Sciences (IRCMS), Kumamoto University, Kumamoto, Japan;* [5]*Department of Molecular Brain Science, Graduate School of Medical Sciences, Kumamoto University, Kumamoto, Japan;* [6]*Department of Obstetrics and Gynecology, Faculty of Life Sciences, Kumamoto University, Kumamoto, Japan;* [7]*Department of Anatomy and Neurobiology, Graduate School of Medical Sciences, Kumamoto University, Kumamoto, Japan;* [8]*Department of Gastroenterology and Hepatology, Mie University, Mie, Japan;* [9]*Department of Pathology, Faculty of Medicine and Graduate School of Medicine, Hokkaido University, Sapporo, Japan;* [10]*Center for Metabolic Regulation of Healthy Aging, Faculty of Life Sciences, Kumamoto University, Kumamoto, Japan*

JHEP Reports **2023.** https://doi.org/10.1016/j.jhepr.2023.100892

Background & Aims: Hepatocellular carcinoma (HCC) mainly develops from chronic hepatitis. Metabolic dysfunction-associated steatohepatitis (MASH) has gradually become the main pathogenic factor for HCC given the rising incidence of obesity and metabolic diseases. 15-Hydroxyprostaglandin dehydrogenase (15-PGDH) degrades prostaglandin 2 (PGE2), which is known to exacerbate inflammatory responses. However, the role of PGE2 accumulation caused by 15-*PGDH* downregulation in the development of MASH-HCC has not been determined.

Methods: We utilised the steric animal model to establish a MASH-HCC model using wild-type and 15-*Pgdh*$^{+/-}$ mice to assess the significance of PGE2 accumulation in the development of MASH-HCC. Additionally, we analysed clinical samples obtained from patients with MASH-HCC.

Results: PGE2 accumulation in the tumour microenvironment induced the production of reactive oxygen species in macrophages and the expression of cell growth-related genes and antiapoptotic genes. Conversely, the downregulation of fatty acid metabolism in the background liver promoted lipid accumulation in the tumour microenvironment, causing a decrease in mitochondrial membrane potential and CD8+ T-cell exhaustion, which led to enhanced development of MASH-HCC.

Conclusions: 15-*PGDH* downregulation inactivates immune surveillance by promoting the proliferation of exhausted effector T cells, which enhances hepatocyte survival and proliferation and leads to the development of MASH-HCC.

Impact and implications: The suppression of PGE2-related inflammation and subsequent lipid accumulation leads to a reduction in the severity of MASH and inhibition of subsequent progression toward MASH-HCC.

Introduction

Hepatocellular carcinoma (HCC) accounts for approximately 90% of all liver cancers, and despite breakthroughs in medical and surgical treatment in recent years, its 5-year survival rate is still only 18%, making HCC the second deadliest cancer after pancreatic cancer.[1] More recently, the terms metabolic dysfunction-associated fatty liver disease (MAFLD) and metabolic dysfunction-associated steatohepatitis (MASH) have been introduced to replace the previous nomenclature of non-alcoholic fatty liver disease (NAFLD) and non-alcoholic steatohepatitis (NASH). The adoption of these new terms is widely supported because of their non-stigmatising nature and potential to enhance awareness and patient identification.[2] Moving forward, we will use the terms MAFLD and MASH to refer to what was previously recognised as NAFLD and NASH. MAFLD is a common aetiology of HCC, which is diagnosed in approximately a quarter of the global population given the rising incidence of obesity and metabolic diseases.[3] MAFLD is often associated with other ailments, such as chronic metabolic liver disease, and can progress to more severe forms of liver disease, such as MASH, which is

Keywords: Chronic inflammation; CD8+ T-cell exhaustion; Cyclooxygenase 2; 15-Hydroxyprostaglandin dehydrogenase; Metabolic dysfunction associated steatohepatitis-hepatocellular carcinoma; Nonalcoholic steatohepatitis-hepatocellular carcinoma; Prostaglandin E2.

Received 20 February 2023; received in revised form 9 August 2023; accepted 16 August 2023; available online 23 August 2023

* Corresponding authors. Addresses: Gastrointestinal Cancer Biology, International Research Center for Medical Sciences (IRCMS), Kumamoto University, 2–2-1 Honjo, Chuo-ku, Kumamoto 860–0811, Japan. Tel.: +81-96-373-6864 (T. Ishimoto); and Gastrointestinal Cancer Biology, International Research Center for Medical Sciences (IRCMS), Kumamoto University, 2–2-1 Honjo, Chuo-ku, Kumamoto 860–0811, Japan. Tel.: +81-96-373-6864 (T. Yasuda).

E-mail addresses: taka1516@kumamoto-u.ac.jp (T. Ishimoto), kumasyuwa@gmail.com (T. Yasuda).

accompanied by severe hepatocellular injury with steatosis characterised by inflammation and ballooning. At least 25% of MAFLD cases are believed to develop into MASH.[4,5]

Many reports have shown that chronic precancerous inflammation or tumour microenvironment (TME)-related inflammation caused by tumour cells plays a "combustion-supporting" role in cancer development, which is one of the characteristics of cancer progression.[3,6] Long-term chronic inflammation can lead to the accumulation of inflammatory cells and mediators in hepatic tissues. Prostaglandin E2 (PGE2) is an important mediator involved in inflammation and is synthesised from arachidonic acid by cyclooxygenase 2 (COX-2). PGE2 participates in various inflammatory activities in the human body[7] and contributes to tumour initiation and progression.[8] 15-Hydroxyprostaglandin dehydrogenase (15-PGDH) is an enzyme that degrades PGE2 and a tumour suppressor located upstream of the COX2/PGE2 signalling pathway.[9] Although several studies have shown the functions of 15-PGDH in cancer tissue,[10,11] the impact of 15-PGDH on the occurrence of MASH-HCC remains unknown.

The advent of immunotherapy, which aims to reactivate antitumour T cells, has revolutionised cancer treatment.[12] Although nivolumab and pembrolizumab have been approved for the treatment of advanced HCC, a recent study revealed that in MASH-HCC, anti-programmed death receptor (PD-1) drugs conversely promote HCC development resulting from an impairment of immune surveillance and induction of MASH-related aberrant CD8+ T-cell activation, which causes tissue damage.[13] Although MASH-HCC progression undoubtedly involves an inflammatory response and inflammatory signalling, it is unclear whether PGE2 signalling has an important role in CD8+ T-cell activation during MASH-HCC development. The present study was conducted to explore the relationship between PGE2 accumulation caused by 15-PGDH downregulation and MASH-HCC development mediated by inflammatory signalling.

Materials and methods

Patients and tissue samples

A total of 1,273 patients with HCC who underwent radical hepatectomy at Kumamoto University Hospital (Kumamoto, Japan) between April 2000 and December 2015 were initially enrolled. Among the 1,273 patients with HCC, 1,125 patients with viral hepatitis and 48 patients who reported alcohol consumption of ≥20 g/day for women and ≥30 g/day for men were excluded based on the MAFLD/MASH criteria. Ultimately, 100 patients with MASH-HCC were eligible for this study. H&E staining and immunohistochemical (IHC) staining were performed on liver resection specimens from eligible patients. Preoperative blood test data and survival information were obtained from patient medical records. All patients signed an informed consent form prior to participation in this study, and the study was approved by the Medical Ethics Committee of Kumamoto University (IRB approval number: 1291).

Animal statement and steric animal model (STAM) mouse model

All animal studies were designed in accordance with the Declaration of Helsinki and were approved by the Kumamoto University Ethics Committee for Animal Experiments (Approval number: A28-052). Efforts were made to meet the scientific goals of this study with a minimum number of animals. Mice were randomly assigned to the control and experimental groups for subsequent drug treatment. MASH-HCC was induced in male mice by a single subcutaneous injection of 100 μg STZ (Catalogue #S0130, Lot #031M1287 V; Sigma–Aldrich) solution (50 mg/ml) 2 days after birth, followed by feeding a high-fat diet (HFD; 57 kcal% fat, Catalogue #HFD32; CLEA Japan Inc, Japan) available *ad libitum* from 4 to 15–20 weeks of age; the mice were euthanized when 15- and 20-weeks-old. The sequence of the 15-*Pgdh*-deficient mouse gRNA we used to generate a 15-*Pgdh*-deficient line was as follows: 5′-TGCTCCATGGCGCCAAGGTA-3′; the target site was located between exon 1 and intron 1 of the 15-*Pgdh* gene.[14] Homozygous mice carrying the 15-*Pgdh* mutant allele were crossed with wild-type (WT) mice to obtain 15-*Pgdh*–heterozygous mice. We utilised 15-$Pgdh^{+/-}$ littermates and 15-$Pgdh^{+/+}$ littermates as the wild-type (WT) control groups.

Evaluation of the MAFLD activity score

The activity of MASH/MAFLD was evaluated using the MAFLD activity scoring system (MAS). Briefly, the MAS comprises four semiquantitative items: steatosis (0–3), lobular inflammation (0–2), hepatocellular ballooning (0–2), and fibrosis (0–4).[15] MAS was generated by evaluating H&E-stained slides.

Immunostaining and scoring methods

Paraffin-embedded sections (4 μm) obtained from patients with MASH-HCC or STAM mice were deparaffinised and soaked in distilled water. Autoclave-induced antigen retrieval was performed. Endogenous peroxidase activity was blocked using 3% hydrogen peroxide. Sections were incubated with primary antibodies against 15-PGDH (ab187161, Abcam), CD86 (#19589, Cell Signalling Technology, Trask Lane, Danvers, MA), CD163 (ab182422, Abcam), Ki-67 (AB_11219741, Spring Bioscience, Pleasanton, CA, USA) overnight at 4 °C. The sections were subsequently incubated with a biotin-free HRP enzyme-labelled polymer using the Envision Plus detection system (Dako, Tokyo, Japan) for 1 h at room temperature. Positive reactions were visualised using a diaminobenzidine solution, followed by counterstaining with Mayer's haematoxylin. All immunohistochemistry (IHC) staining was scored by both the intensity and percentage of cell staining. The average intensity of positively stained cells was given an intensity score from 0 to 3 (0: none, 1: weak, 2: moderate, and 3: strong expression). The average proportion of positively stained cells was estimated and given a percentage score on a scale from 1 to 6 (1, 0–5%; 2, 6–20%; 3. 21–40%; 4, 41–60%; 5, 61–80%, and 6, 81–100%). The two scores were multiplied to characterise 15-PGDH, CD163, CD86, PD-1 and Ki-67 expression as low (0-7) or high (8–18). Sirius Red staining was performed to assess liver fibrosis. Briefly, sections were stained with a 0.1% Sirius Red-1.3% picric acid solution (Muto Pure Chemicals Co. Ltd., 33061, Japan) and quickly rinsed with acetic acid (0.5%). The positively stained area was measured as a percentage. All scoring assessments were performed independently by two investigators.

Oil Red O staining

Adipocytes and neutral fat were stained with an Oil Red O stock solution (Muto Pure Chemicals Co., Ltd, 40491, Japan). Briefly,

frozen mouse liver sections (15 μm) were incubated with 1 ml of Oil Red O solution (Oil Red O stock solution: distilled water = 6:4) for 15 min at room temperature, washed with 60% isopropanol, stained with a haematoxylin solution to visualise cell nuclei, and finally mounted with a water-based mounting medium.

Preparation of single-cell suspensions

The protocol for cell isolation and fluorescence-activated cell sorting (FACS) analysis using mouse samples was described in a previous study.[16] In brief, livers were surgically excised from 15-week-old STAM mice, minced, and dissociated in medium containing Dri Tumor & Tissue Dissociation Reagent (BD Horizon™, USA) according to the manufacturer's protocol. The cell suspensions were passed through a 70-μm cell strainer (CORNING, Falcon, USA), haemolysed with VersaLyse (Beckman Coulter), washed with PBS containing 2% FBS and 2 mM EDTA, and used in subsequent experiments.

Flow cytometry

All cells were adjusted to a density of 1×10^6 cells/100 μl and stained with Fixable Viability Stain 510 (BD Horizon™, USA) prior to surface antibody staining. Purified rat anti-mouse CD16/CD32 (Mouse BD Fc Block™,BD Horizon™, USA) was used for subsequent Fc blocking. Antibodies for surface staining were diluted in PBS containing 2% FBS and 10% mouse serum and incubated for 30 min at 4 °C. The samples were then fixed using fixation buffer (BD Horizon™, USA). For intracellular staining, cells were permeabilised with 1x eBioscience™ Permeabilization Buffer (Thermo Fisher Scientific, USA) for 15 min at room temperature, and then antibodies for intracellular staining were diluted in the same permeabilization buffer and incubated for 30 min at 4 °C. Data acquisition was performed using a BD FACSVerse™ (BD Horizon™, USA), collecting 50,000 FVS510-CD45+ events per sample when possible. FlowJo™ software v10 (BD Horizon™, USA) was used to analyse the acquired data. The antibodies used in this study are listed in Table S1.

Quantitative reverse transcription-PCR

Total RNA was extracted from dissociated cells using the miRNeasy Mini Kit (Qiagen, Hilden, Germany) according to the manufacturer's protocol. Complementary DNA (cDNA) was reverse transcribed from the isolated total RNA using SuperScript III, RNaseOUT, Recombinant Ribonuclease Inhibitor, Random Primers and Oligo(dT)12–18 Primer (Thermo Fisher Scientific, USA). mRNA expression was quantified using SYBR Green. Reactions were performed using a LightCycler 480 System II (Roche Diagnostics, Belarus). All qRT–PCR data are displayed as the means ± standard errors (SEs) of the mean. The primer sequences are listed in Table S2.

Western blotting analysis

Homogenised cells from the background liver of STAM mice were lysed with RIPA buffer containing a protease and phosphatase inhibitor cocktail (Thermo Fisher Scientific, USA). The lysate was sonicated, debris was removed by centrifugation, and the supernatant was collected as the whole-cell lysate. Protein samples were subjected to SDS–PAGE, transferred to polyvinylidene difluoride membranes, and blotted with primary antibodies (ab187161, Abcam) in Can Get Signal Solution 1 (Toyobo) at 4 °C overnight. Signals were detected after incubation with anti-rabbit or anti-mouse secondary antibodies in Can Get Signal Solution 2 at room temperature for 1 h using an ECL Detection System (GE Healthcare, Little Chalfont, Buckinghamshire, UK). Band signals were quantified with ImageJ software (ImageJ, RRID: SCR_003070).

ELISA

The protein levels of PGE2 were measured by a PGE2-EIA Monoclonal Kit (Cayman Chemical Company, USA) using conditioned medium. The assay procedure followed the manufacturer's protocol.

Monocyte isolation, macrophage induction, and reactive oxygen species assay

Peripheral blood mononuclear cells (PBMCs) were isolated from fasting blood samples collected from healthy human donors. Subsequently, monocytes were isolated from the PBMCs by immunomagnetic negative selection using the EasySep™ Human Monocyte Enrichment Kit (StemCell Technologies, Canada). To induce M0 macrophages, isolated monocytes were suspended in RPMI 1640 medium containing 10% heat-inactivated FBS and 50 ng/ml M-CSF (PeproTech, USA) and incubated at 37 °C with 5% CO_2. During differentiation culture, the medium was replaced with the same medium every 2–3 days, and M0 macrophages were induced for 7 days. The induced cells were detached with EDTA-trypsin on Day 7 and incubated overnight after seeding at 1×10^6 cells/ml. On Day 8, the medium was changed to medium containing 100 pM PGE2 (Cyman No. 14010, USA), and after treatment for 6 h, reactive oxygen species (ROS) were labelled using the DCFDA-Cellular ROS Assay Kit (Abcam) according to the manufacturer's protocol. Labelled ROS were measured and analysed via flow cytometry and FlowJo software as described above.

DNA isolation, whole-exome sequencing, and sequence alignment

Genomic DNA was isolated from background liver tissue using a DNeasy Blood & Tissue kit (Qiagen, Hilden, Germany) according to the manufacturer's instructions. Exome capture libraries were prepared following the instructions of the SureSelectXT mouse all exon target enrichment system (Agilent Technologies). The exome libraries were sequenced using a 125-base pair paired-end read protocol on an Illumina HiSeq 2500. Sequencing reads were trimmed using Cutadapt (v1.18) and Trimmomatic (v0.39) and aligned to the reference genome GRCm38 (mm10) using BWA (v0.7.17). Aligned reads were marked as duplicates using Picard (v2.18.21) and SAMtools (v1.11), followed by base recalibration using GATK (v4.1.1.0). The whole-exome sequencing data were deposited in the DDBJ database under accession number DRA016752.

Variant identification and mutational signature analyses

Single-nucleotide variants (SNVs) and indel variants were called using Mutect2 (v4.1.1.0). No normal tail DNA samples corresponding to the background liver samples were obtained in this analysis. Therefore, normal liver samples from untreated 15-*Pgdh*$^{+/-}$ mice (n = 3) were used as a control sample for comparison to the samples from 15-*Pgdh*$^{+/-}$ (n = 3) and 15-*Pgdh*$^{+/-}$ (n = 6)

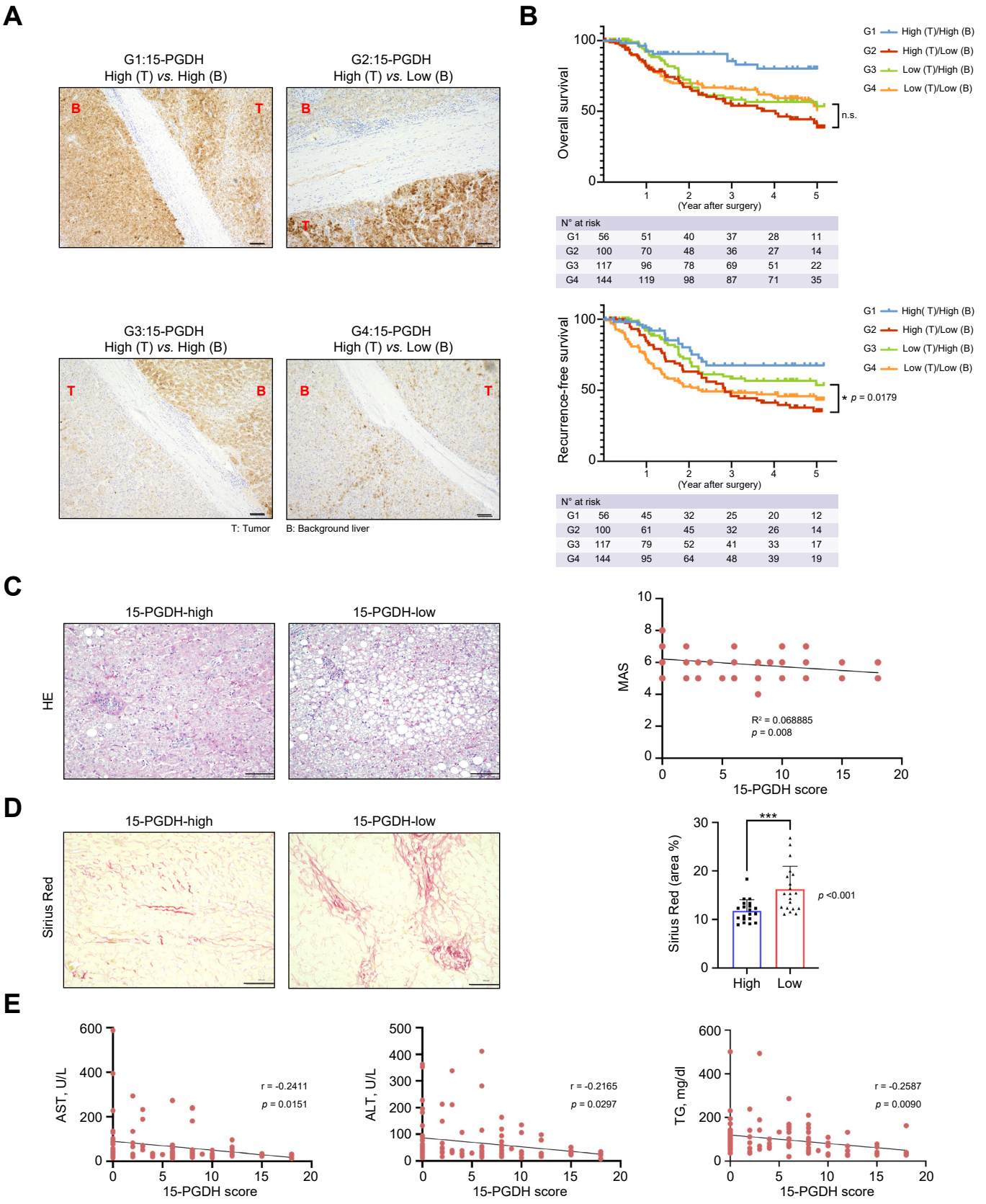

Fig. 1. Low expression of 15-PGDH in the background liver indicates an increased recurrence rate for HCC and elevated MASH activity in patients with MASH-HCC. (A) Representative IHC staining for 15-PGDH in the 4 groups (tumour:background = high:high (Group 1), high:low (Group 2), low:high (Group 3), low:low (Group 4)). Scale bars, 100 μm. (B) OS and RFS of patients with MASH-HCC stratified into 4 groups. (C) Representative H&E staining of the background liver of patients with MASH-HCC with high or low expression of 15-PGDH and the correlation between the MAS and 15-PGDH expression score. (D)

STAM mice for SNV/indel detection with Mutect2. SNVs/indels were filtered and annotated using SnpShift & SnpEff (v5.1). GRCm38.74 obtained using SnpEff was used for the annotation file. Nonsynonymous SNVs were confirmed by visual inspection of aligned reads with IGV (v2.4.14). Mutation signature profiling and fitting to SBS was performed using MutationalPatterns (v3.6.0).[17]

RNA sequencing

RNA sequencing was performed following the established protocol described in a previous study conducted at Kumamoto University (Kumamoto, Japan). The sequencing procedure was performed by the Liaison Laboratory Research Promotion Center at Kumamoto University. Total RNA was isolated using the RNeasy Mini Kit (catalogue no. 74106, Qiagen, Hilden, Germany), and the concentration and purity of the RNA were assessed using an Agilent 2100 bioanalyzer (Agilent). Only samples with an RNA integrity number (RIN) greater than 8.0 were selected for sequencing. For the sequencing analysis, a NextSeq 500 platform (Illumina) was utilised, and the obtained data were converted to the Fastq format for further analysis. The quality of the data was determined by Trim galore (v0.5.0). The filtered reads were then mapped to the GRCm38 reference genome using STAR (v2.6.0). Transcripts per million mapped reads (TPM) values were calculated using RSEM. The RNA-sequencing data were deposited in the DDBJ database under accession number DRA016740. The R package: DESeq2 (1.36.0) and edge (v3.38.2) were used to analyse the differentially expressed genes (DEG) between two groups of STAM mice and the R package ggplot2 (v3.3.6) and Complex Heatmap (2.13.1) were used to visualise the difference analysis results. *P* values <0.05 and |log2 FC| >1.5) were set as the cut-off criteria and considered to indicate statistical significance. After performing ID conversion on the input molecule list (ID conversion library package: org.Hs.eg.db), the cluster Profiler package (ver.4.4.4) was used for enrichment analysis and ggplot2 (v3.3.6) for visualisation (R v4.2.1).

Analysis of Liver Cell Atlas and published datasets

The Liver Cell Atlas is a public database based on published liver single-cell RNA sequencing datasets for humans and mice generated in the laboratories of Charlotte Scott and Martin Guilliams from the VIB-UGent Centre for Inflammation Research, Belgium (https://www.livercellatlas.org/index.php). The 15-*PGDH* gene (official symbol, *HPGD*) was selected, and the distribution of mRNA expression in all human and mouse liver cells was analysed.

Fluorescently labelled long-chain fatty acid treatment

Mice were injected intraperitoneally with 50 μg of fluorescently labelled long-chain fatty acid (LCFA), specifically BODIPY FL C16 (Thermo Fisher Scientific, USA), in 50 μl of DMSO. The mice were euthanized 1 h after the treatment, and single-cell suspensions were prepared from the mouse background liver as described above. CD8+ T cells were then isolated from single-cell suspensions using the EasySep™ Mouse CD8+ T Cell Isolation Kit (StemCell Technologies, Canada), and BODIPY-C16+CD8+ T cells were quantified by flow cytometry.

Palmitoleic acid (Plam) and oleic acid (Ole) treatment, cell counting, and cell trace assay

CD8+ T cells were freshly isolated from single-cell suspensions of splenocytes from WT mice using the EasySep™ Mouse CD8+ T-Cell Isolation Kit (StemCell Technologies, Canada). The isolated CD8+ T cells were cultured in 96-well microplates in complete medium supplemented with Palmitoleic acid (Palm) / oleic acid or a mixture of Palm and (BSA-Oleate (Sigma–Aldrich, UAS) at 100 μM from Days 1 to 7. The CFSE assay was performed using the CellTrace™ Violet Cell Proliferation Kit (Thermo Fisher Scientific, USA) according to the manufacturer's protocol. Cell Trace Violet fluorescence detection and cell counting were performed by flow cytometry. The data were analysed using FlowJo software. During this culture experiment, T-cell activity was maintained with mouse interleukin (IL)-2 (BioLegend, CA, USA) (100 μg/ml for the cell counting assay, 50 μg/ml for the cell trace assay) and Dynabeads™ Mouse T-Activator CD3/CD28 for T-Cell Expansion and Activation (Thermo Fisher Scientific, USA).

Measurement of the T-cell mitochondrial membrane potential

T cells isolated from the spleen or liver were treated with or without Tissue Dissociation Reagent (sBD Horizon™, USA) for 10 min and then stained with 2 μM JC-1 and 10 μM CCCP as a positive control for 30 min at room temperature for measurement of the mitochondrial membrane potential. FACS analyses were performed using a Symphony flow cytometer (sBD Horizon™, USA). The data were analysed using FlowJo software.

Statistical analysis

All experiments were performed in triplicate, and the data shown are representative of consistent results. Data are presented as the mean ± SE. The Mann–Whitney *U* test was used to compare continuous variables between two groups. Categorical variables were compared using the χ^2 test. Correlations were evaluated by Pearson's correlation coefficient analysis. Survival curves were generated using the Kaplan–Meier method, and the log-rank test was performed for survival analysis. Statistical significance was defined as *p* values <0.05, and all data met the assumptions of the statistical test used for distribution and variance. Variance was not statistically significant in any of the results. No statistical method was used to predetermine the sample size for any of the *in vitro* or *in vivo* experiments. All statistical analyses were performed with SPSS (v26, IBM Corp.) and Prism software (v9.0.1, GraphPad, USA).

Representative Sirius Red staining of the background liver of patients with MASH-HCC with high or low expression of 15-*PGDH* and quantitative comparison of the Sirius Red-positive areas between the groups of patients with MASH-HCC with high or low expression of 15-*PGDH* in the background liver (n = 10/group). (E) Pearson's correlations of 15-*PGDH* expression in the background liver with preoperative serum AST, ALT, and TG levels in patients with MASH-HCC. **p* <0.05, ***p* <0.01 Mann–Whitney *U* test. 15-PGDH, 15-hydroxyprostaglandin dehydrogenase; ALT, alanine aminotransferase; AST, aspartate aminotransferase; HCC, hepatocellular carcinoma; IHC, immunohistochemistry; MAFLD, metabolic dysfunction associated fatty liver disease; MAS, MAFLD activity score (MAS); MASH, metabolic dysfunction associated steatohepatitis; ns, not significant; OS, overall survival (OS); RFS, recurrence-free survival (RFS); TG, triglycerides.

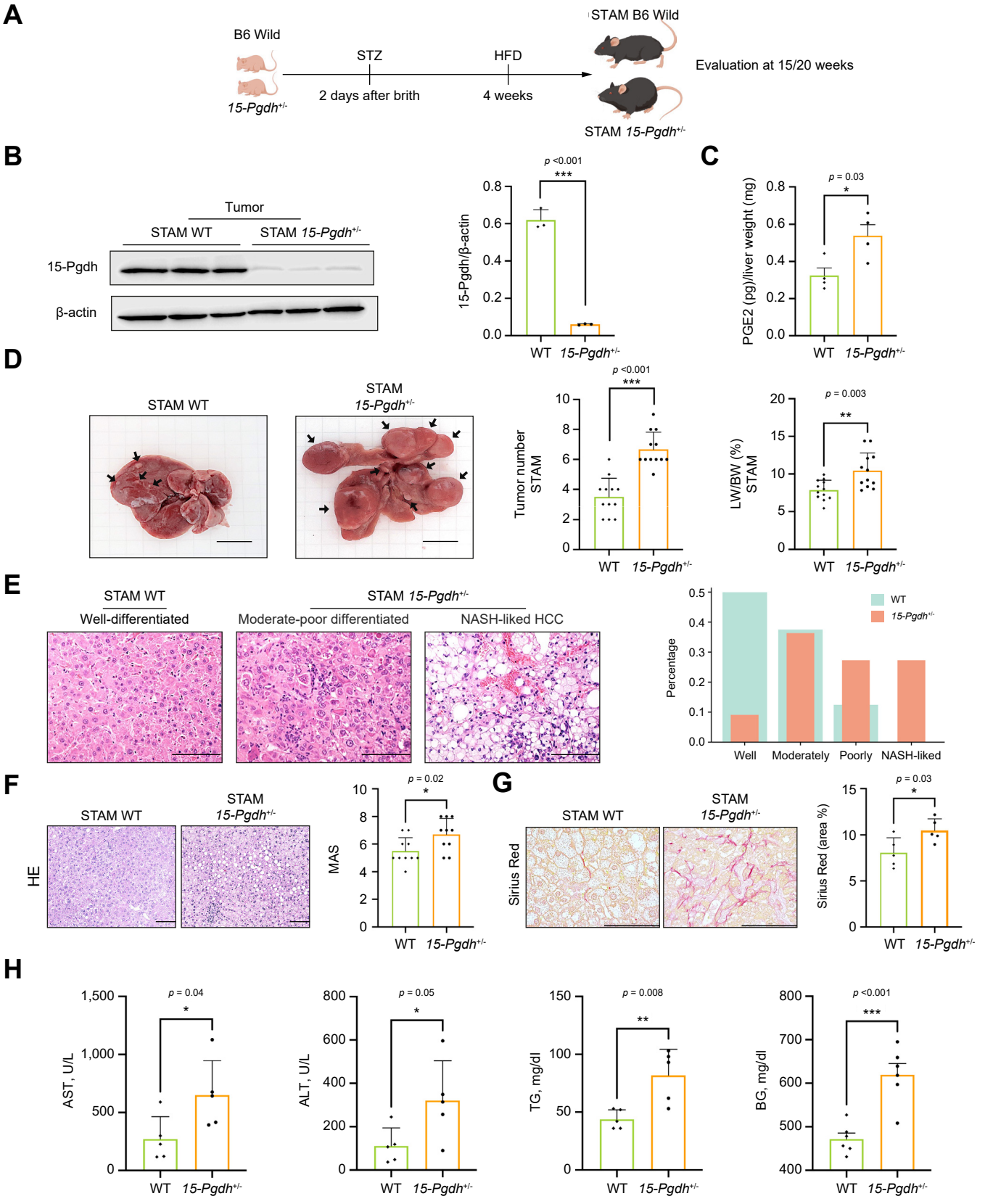

Fig. 2. MASH-HCC incidence and MASH activity are accelerated in STAM 15-*Pgdh*$^{+/-}$ mice. (A) Schematic timeline of the development of the STAM with wild-type and 15-*Pgdh*$^{+/-}$ mice. (B) Western blotting analysis of 15-Pgdh protein levels in liver tissue from STAM WT and 15-*Pgdh*$^{+/-}$ mice. The graph represents normalisation of 15-Pgdh to total B-actin (n = 3/group). (C) PGE2 expression was measured by ELISA in STAM WT and 15-*Pgdh*$^{+/-}$ mice. (D) Representative images of liver tumours from STAM WT and 15-*Pgdh*$^{+/-}$ mice. The graph represents the number of visible tumours and the ratio of liver weight to body weight (LW/BW) in

For further details regarding the materials used, please refer to the CTAT table.

Results

Patients with MASH-HCC with 15-PGDH downregulation in the background liver showed a higher NAS and an increased recurrence rate

We first selected 100 patients with MASH-HCC from a total cohort of 1273 patients with HCC who underwent radical hepatic resection by excluding 1125 patients with viral hepatitis and 48 patients with a long-term history of alcohol consumption. We then performed IHC staining of liver tissues from 100 patients with MASH-HCC to evaluate the expression of 15-*PGDH* using the tumour area or peritumour area (background liver) of each sample. Based on the expression of 15-*PGDH*, both the tumour area and the background liver area of the 100 MASH-HCC samples were classified into 4 groups: tumour:background = high:-high (Group 1, n = 56), high:low (Group 2, n = 100), low:high (Group 3, n = 117), and low:low (Group 4, n = 144) (Table S1, Fig. 1A, Fig. S1A).

We subsequently assessed the relationship between the 5-year overall survival (OS) or the recurrence-free survival (RFS) of patients with MASH-HCC and the expression levels of 15-PGDH in the tumour area or background liver by Kaplan–Meier analysis. Groups 2, 3, and 4, which were defined as patients with 15-PGDH–low expression regardless of the tumour and background liver, exhibited significantly shorter OS than that of Group 1. Groups 2 and 3 showed no significant differences in OS. Conversely, Group 2, which was defined as 15-PGDH–low only in the background liver, showed a significantly shorter RFS than that of Group 3 (Group 2 RFS: 12.0% *vs*. Group 3 14.53%, p = 0.0179). This finding suggests that when defined according to the background liver expression, the downregulation *PGDH* is associated with the occurrence of MASH-HCC (Fig. 1B).

Given the RFS outcomes determined by Kaplan–Meier analysis, we further examined the importance of *15-PGDH* expression in the background liver of patients with MASH-HCC. We first compared MAFLD activity in the background liver of 15-PGDH–high and 15-PGDH–low groups of patients MASH-HCC using the MAS. The expression level of 15-PGDH was inversely correlated with the MAS, and the liver fibrosis evaluated by Sirius Red staining was higher in the 15-PGDH–low group than in the 15-PGDH–high group (Fig. 1C and D). Moreover, the levels of aspartate aminotransferase (AST), alanine aminotransferase (ALT), and triglycerides (TG) in the preoperative blood samples were significantly higher in the 15-PGDH–low group than in the 15-PGDH–high group (Fig. 1E). These findings suggest that 15-PGDH downregulation in the background liver is correlated with MASH-HCC occurrence and promotes MAFLD activity.

Moreover, according to the evaluation of the expression of 15-PGDH in specimens exhibiting steatosis, fibrosis (background liver) and at tumour sites, we found that the expression of 15-PGDH in patients varied depending on their inflammatory status. To further investigate this notion, we analysed 15-*PGDH* mRNA expression using a public dataset from a previous study.[18] This analysis focused on HCV-infected patient datasets to assess the association with inflammation status more clearly. Our analysis demonstrated a gradual decrease in 15-*PGDH* expression according to the METAVIR Activity Grade, a score based on the degree of inflammation and fibrosis. This finding provides additional support for the association between the downregulation of 15-*PGDH* and inflammation (Fig. S1B). These findings emphasise the importance of considering the inflammation status derived from the downregulation of 15-PGDH.

MAFLD activity and MASH-HCC incidence were increased in STAM 15-*Pgdh*$^{+/-}$ mice

To elucidate the significance of 15-PGDH downregulation in MASH-HCC development, we first investigated the distribution of 15-PGDH mRNA expression in all human and mouse liver cells from the Liver Cell Atlas, which is a public database based on published liver single-cell RNA sequencing datasets for humans and mice. In the human liver, the 15-*PGDH* gene is primarily expressed in hepatocytes, with only limited expression in different immune cell types, such as T cells and basophils. Conversely, in mice, the 15-*Pgdh* gene is expressed broadly, although hepatocytes remain one of the major sources of its expression (Fig. S2A–D). In our previous study, we examined the impact of 15-*Pgdh* expression from macrophages in a mouse model of pancreatic cancer. 15-*Pgdh* deficiency in macrophages caused tumour proliferation and enhanced fibrosis.[19] Therefore, we utilised 15-*Pgdh*-deficient mice (15-*Pgdh*$^{+/-}$, 15-*Pgdh*$^{-/-}$) with whole-body depletion, including hepatocytes and immune cells, which could be more influenced by the expression of 15-*Pgdh*. As we described in a previous report, 15-*Pgdh*$^{-/-}$ mice are born with ductus arteriosus, and indomethacin treatment rescued these mice after birth; however, the successful rescue rate was extremely low.[19] Almost all 15-*Pgdh*$^{-/-}$ mice died after 2 to 4 weeks during the process of MASH induction; therefore, we decided to examine MASH-HCC development in 15 *Pgdh*$^{+/-}$ mice in the present study. Moreover, we used the STAM to establish a MASH-HCC model using WT and 15-*Pgdh*$^{+/-}$ mice following a previous report (Fig. 2A).[20] Western blotting analysis confirmed that the expression of 15-*Pgdh* in liver tissues from STAM 15-Pgdh $^{+/-}$ mice was significantly downregulated (Fig. 2B). Next,

each group (n = 12). Scale bars, 100 μm. (E) Representative H&E staining of well-differentiated HCC from STAM WT mice and moderately to poorly differentiated/MASH-like HCC from STAM 15-*Pgdh*$^{+/-}$ mice. The graph represents the percentage of tumours grouped by tumour differentiation stage in each group. The STAM WT group included the evaluation of 12 tumours from STAM WT mice (n = 6). The STAM 15-*Pgdh*$^{+/-}$ group included the evaluation of 11 tumours from STAM 15-*Pgdh*$^{+/-}$ mice (n = 4). Scale bars, 100 μm. (F) Representative H&E staining of the background liver of STAM WT and 15-*Pgdh*$^{+/-}$ mice. The graph represents the MAS values in each group (n = 10). Scale bars, 100 μm. (G) Representative Sirius Red staining of the background liver of STAM WT and 15-*Pgdh*$^{+/-}$ mice. The graph represents the quantification of Sirius Red-positive areas for each group (n = 5). Scale bars, 100 μm. (H) AST, ALT, TG, and blood glucose (BG) levels in peripheral blood from STAM WT and 15-*Pgdh*$^{+/-}$ mice collected at 20 weeks of age (AST, ALT, TG: n = 5; BG: n = 6). *p <0.05, **p <0.01 Mann–Whitney *U* test. 15-PGDH, 15-hydroxyprostaglandin dehydrogenase; ALT, alanine aminotransferase; AST, aspartate aminotransferase; BG, blood glucose; HCC, hepatocellular carcinoma; LW/BW, ratio of liver weight to body weight; MASH, MASH, metabolic dysfunction associated steatohepatitis; MAS, MAFLD activity score; n.s., not significant; STAM, steric animal model; TG, triglycerides; WT, wild-type.

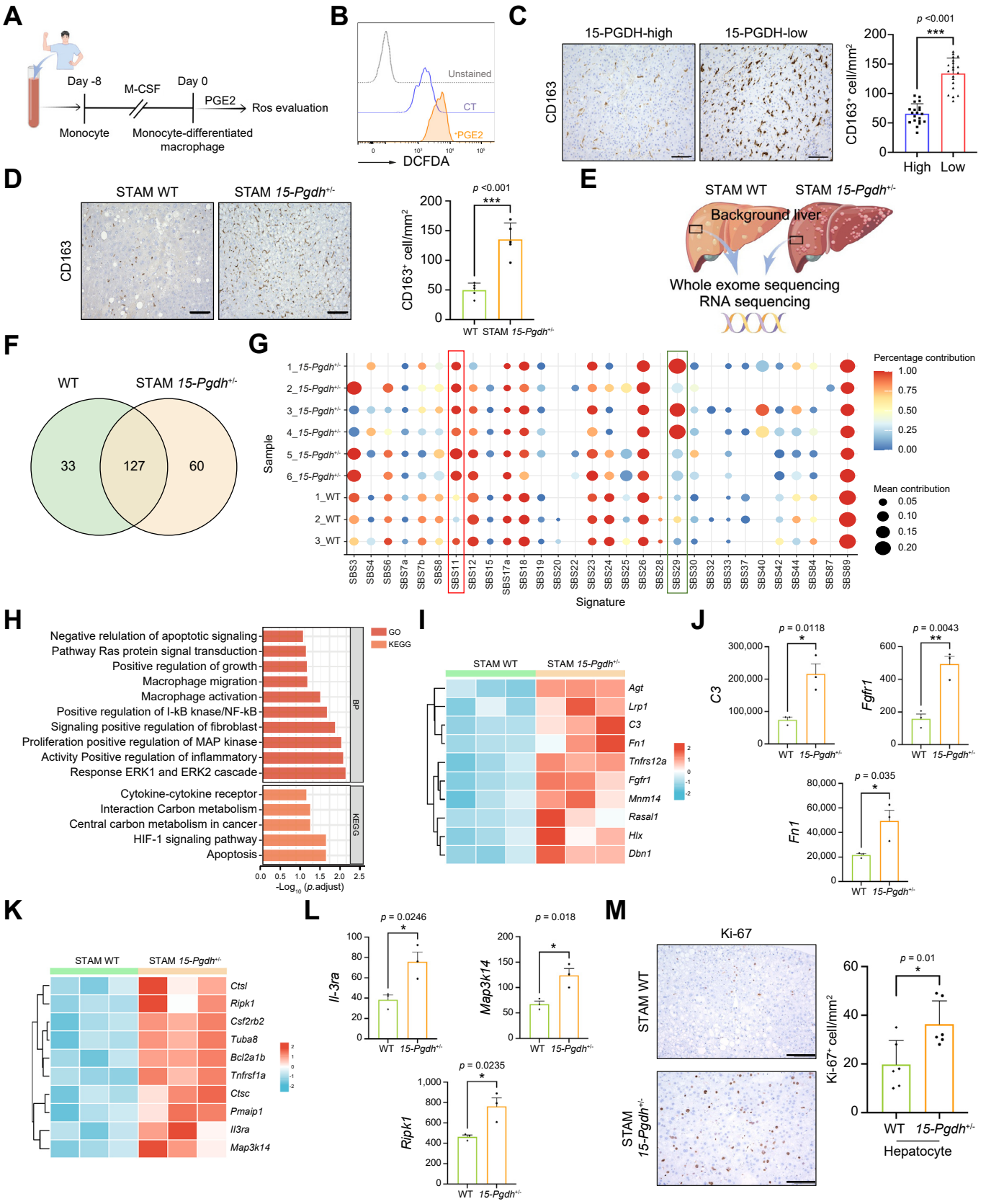
A
Day -8
M-CSF
Day 0
PGE2
Ros evaluation
Monocyte
Monocyte-differentiated macrophage
B
Unstained
CT
PGE2
DCFDA
C
15-PGDH-high
15-PGDH-low
CD163
p <0.001
***
CD163+ cell/mm2
High
Low
D
STAM WT
STAM 15-Pgdh+/-
CD163
p <0.001
***
CD163+ cell/mm2
WT
STAM 15-Pgdh+/-
E
STAM WT
STAM 15-Pgdh+/-
Background liver
Whole exome sequencing
RNA sequencing
F
WT
STAM 15-Pgdh+/-
33
127
60
G
Sample
1_15-Pgdh+/-
2_15-Pgdh+/-
3_15-Pgdh+/-
4_15-Pgdh+/-
5_15-Pgdh+/-
6_15-Pgdh+/-
1_WT
2_WT
3_WT
SBS3
SBS4
SBS6
SBS7a
SBS7b
SBS8
SBS11
SBS12
SBS15
SBS17a
SBS18
SBS19
SBS20
SBS22
SBS23
SBS24
SBS25
SBS26
SBS28
SBS29
SBS30
SBS32
SBS33
SBS37
SBS40
SBS42
SBS44
SBS84
SBS87
SBS89
Signature
Percentage contribution
1.00
0.75
0.50
0.25
0.00
Mean contribution
0.05
0.10
0.15
0.20
H
Negative relulation of apoptotic signaling
Pathway Ras protein signal transduction
Positive regulation of growth
Macrophage migration
Macrophage activation
Positive regulation of I-kB knase/NF-kB
Signaling positive regulation of fibroblast
Proliferation positive regulation of MAP kinase
Activity Positive regulation of inflammatory
Response ERK1 and ERK2 cascade
Cytokine-cytokine receptor
Interaction Carbon metabolism
Central carbon metabolism in cancer
HIF-1 signaling pathway
Apoptosis
GO
KEGG
BP
KEGG
-Log10 (p.adjust)
I
STAM WT
STAM 15-Pgdh+/-
Agt
Lrp1
C3
Fn1
Tnfrs12a
Fgfr1
Mnm14
Rasal1
Hlx
Dbn1
J
C3
p = 0.0118
WT
15-Pgdh+/-
Fgfr1
p = 0.0043
Fn1
p = 0.035
K
STAM WT
STAM 15-Pgdh+/-
Ctsl
Ripk1
Csf2rb2
Tuba8
Bcl2a1b
Tnfrsf1a
Ctsc
Pmaip1
Il3ra
Map3k14
L
Il-3ra
p = 0.0246
Map3k14
p = 0.018
Ripk1
p = 0.0235
M
Ki-67
STAM WT
STAM 15-Pgdh+/-
p = 0.01
Ki-67+ cell/mm2
WT
15-Pgdh+/-
Hepatocyte

we examined the accumulation of PGE2 protein in both types of STAM mice using ELISA. As expected, PGE2 was significantly accumulated in STAM 15-*Pgdh*$^{+/-}$ mice (Fig. 2C). The number of visible tumours and the liver weights of STAM 15-*Pgdh*$^{+/-}$ mice with MASH-HCC induction for 20 weeks were significantly increased compared with those of STAM WT mice (Fig. 2D). In contrast, 15-*Pgdh*$^{+/-}$ mice fed only a HFD for 20 weeks had significantly increased liver weight but not an increased occurrence of HCC (Fig. S2E). Moreover, from a pathological perspective, the proportion of poorly differentiated tumours was increased in STAM 15-*Pgdh*$^{+/-}$ mice compared with STAM WT mice, and MASH-like HCC was detected only in the liver tissues of STAM 15-*Pgdh*$^{+/-}$ mice (Fig. 2E).

We also assessed the MAFLD activity of the background liver. Consequently, we found that the MAS and the level of fibrosis were higher in the STAM 15-*Pgdh*$^{+/-}$ mice than in the STAM WT mice (Fig. 2F and G). Biochemical examination of peripheral blood samples revealed that the levels of AST, ALT, TG, and blood glucose (BG) were significantly higher in the STAM 15-*Pgdh*$^{+/-}$ mice than in STAM WT mice (Fig. 2H). These findings strongly support the hypothesis that the accumulation of PGE2 through 15-*PGDH* downregulation in the background liver promotes MAFLD activity and the incidence of MASH-HCC.

Increased gene expression related to cell growth and antiapoptotic processes could enhance hepatocyte growth in STAM 15-*Pgdh*$^{+/-}$ mice

To identify the molecular mechanisms by which 15-*PGDH* downregulation promotes MASH-HCC development, we focused on the relationship between PGE2 accumulation and inflammatory responses in the liver. Based on recent evidence indicating that in chronic inflammation, macrophage mitochondria can produce large amounts of ROS, which can induce DNA damage and M2 polarisation,[21,22] we hypothesised that the accumulation of PGE2 caused by 15-PGDH downregulation induces ROS production in macrophages followed by DNA damage in hepatocytes. Thus, we first examined whether the accumulation of PGE2 could induce an increase in mitochondrial ROS production by macrophages *in vitro*. We extracted monocytes from peripheral blood samples collected from healthy human donors and induced M0 macrophages. We then treated M0 macrophages with PGE2 and detected ROS levels using DCFDA (Fig. 3A). The results showed that ROS levels in macrophages treated with PGE2 were significantly higher than those in untreated macrophages (Fig. 3B). We next evaluated macrophages in the background liver of patients with MASH-HCC using an M1-like macrophage-specific marker (CD86) and an M2-like macrophage-specific marker (CD163). The results indicated a significant increase only in the levels of M2-like macrophages in patients with MASH-HCC in the 15-PGDH–low group compared with patients in the 15-PGDH–high group (Fig. 3C and Fig. S3A). Correspondingly, we observed a significant increase only in M2-like macrophages (CD163) in STAM 15-Pgdh$^{+/-}$ mice compared with STAM WT mice (Fig. 3D and Fig. S3B). Moreover, our analysis revealed a correlation between CD163 expression and the downregulation of 15-*PGDH* in patients with MASH-HCC, whereas no such correlation was observed with CD86 expression (Fig. S3C and D). These results suggest that PGE2 accumulation is involved in M2-like macrophage polarisation in the background liver of patients with MASH-HCC.

ROS are a well-known factor responsible for DNA damage and subsequent mutation. Therefore, we next performed whole-exome sequencing using DNA samples extracted from the background liver of STAM mice to investigate whether DNA mutation in hepatocytes is a determining factor in the occurrence of HCC (Fig. 3E). By comparing the number of mutated genes between STAM WT and STAM 15-*Pgdh*$^{+/-}$ mice, we found that the tumour mutational burden was not notably different between the two strains, although the expression of previously reported cancer-related gene signatures (*SBS11* and *SBS29*)[23] were increased in STAM 15-*Pgdh*$^{+/-}$ mice (Fig. 3F and G).

Given that the mutational burden in hepatocytes was not affected by 15-*Pgdh* downregulation, we next conducted a comprehensive gene expression analysis via RNA sequencing of background liver tissues from STAM WT and 15-*Pgdh*$^{+/-}$ mice. Pathway analysis evaluating the differentially expressed genes (DEGs) revealed that gene sets related to cell growth and negative regulation of apoptotic signalling pathways were enriched in STAM 15-*Pgdh*$^{+/-}$ mice compared with STAM WT mice (Fig. 3H). Moreover, the expression of the top 10 upregulated genes in each of the cell growth- and antiapoptotic process-related pathways was markedly higher in the STAM 15-*Pgdh*$^{+/-}$ mice than in the

Fig. 3. Hepatocyte proliferation is enhanced by regulating proliferative and antiapoptotic gene expression in STAM 15-*Pgdh*$^{+/-}$ mice. (A) Schematic diagram of monocyte isolation from the peripheral blood of healthy donors, followed by macrophage induction and subsequent PGE2 treatment. (B) Flow cytometry histogram showing DCFDA staining of monocyte-differentiated macrophages treated with PGE2. (C) Representative IHC staining for CD163 in the background liver of patients with MASH-HCC with high or low expression of 15-*PGDH* (n = 10/group). The graph represents the number of CD163-positive cells per mm^3 in four randomly selected areas. Scale bars, 100 μm. (D) Representative IHC staining for CD163 in the background liver of STAM WT and 15-*Pgdh*$^{+/-}$ mice (n = 6/group). The graph represents the number of CD163-positive cells per mm^3 in four randomly selected areas. Scale bars, 100 μm. (E) Schematic diagram of DNA extraction from the background liver of STAM WT and 15-*Pgdh*$^{+/-}$ mice for WES. (F) The number of gene mutations in the background liver of STAM WT and 15-*Pgdh*$^{+/-}$ mice determined by WES. (G) Mutational landscapes of the background liver of STAM WT and 15-*Pgdh*$^{+/-}$ mice by the COSMIC mutational signature. (H) GO and KEGG pathway enrichment analyses of differentially expressed genes in the background liver of STAM 15-*Pgdh*$^{+/-}$ mice. (I) Heatmap of the top 10 upregulated genes involved in proliferation-related pathways in the background liver of STAM WT and 15-*Pgdh*$^{+/-}$ mice. (J) Validation of the upregulation of selected genes involved in proliferation-related pathways in the background liver of STAM mice by qRT–PCR. (K) Heatmap of the top 10 upregulated genes involved in the anti-apoptotic process-related pathways in the background liver of STAM WT and 15-*Pgdh*$^{+/-}$ mice. (L) Validation of the upregulation of selected genes involved in antiapoptotic process-related pathways in the background liver of STAM mice by qRT–PCR. (M) Representative IHC staining for Ki-67 in the background liver of STAM WT and 15-*Pgdh*$^{+/-}$ mice (n = 6/group). The graph represents the number of Ki-67-positive cells per mm^3 in four randomly selected areas. Scale bars, 100 μm $^*p$ <0.05, $^{**}p$ <0.01 Mann–Whitney *U* test. 15-PGDH, 15-hydroxyprostaglandin dehydrogenase; GO, Gene Ontology; IHC, immunohistochemistry; KEGG, Kyoto Encyclopedia of Genes and Genomes; MASH, metabolic dysfunction-associated steatohepatitis; PGE2, Prostaglandin E2; STAM, steric animal model; WES, whole-exome sequencing.

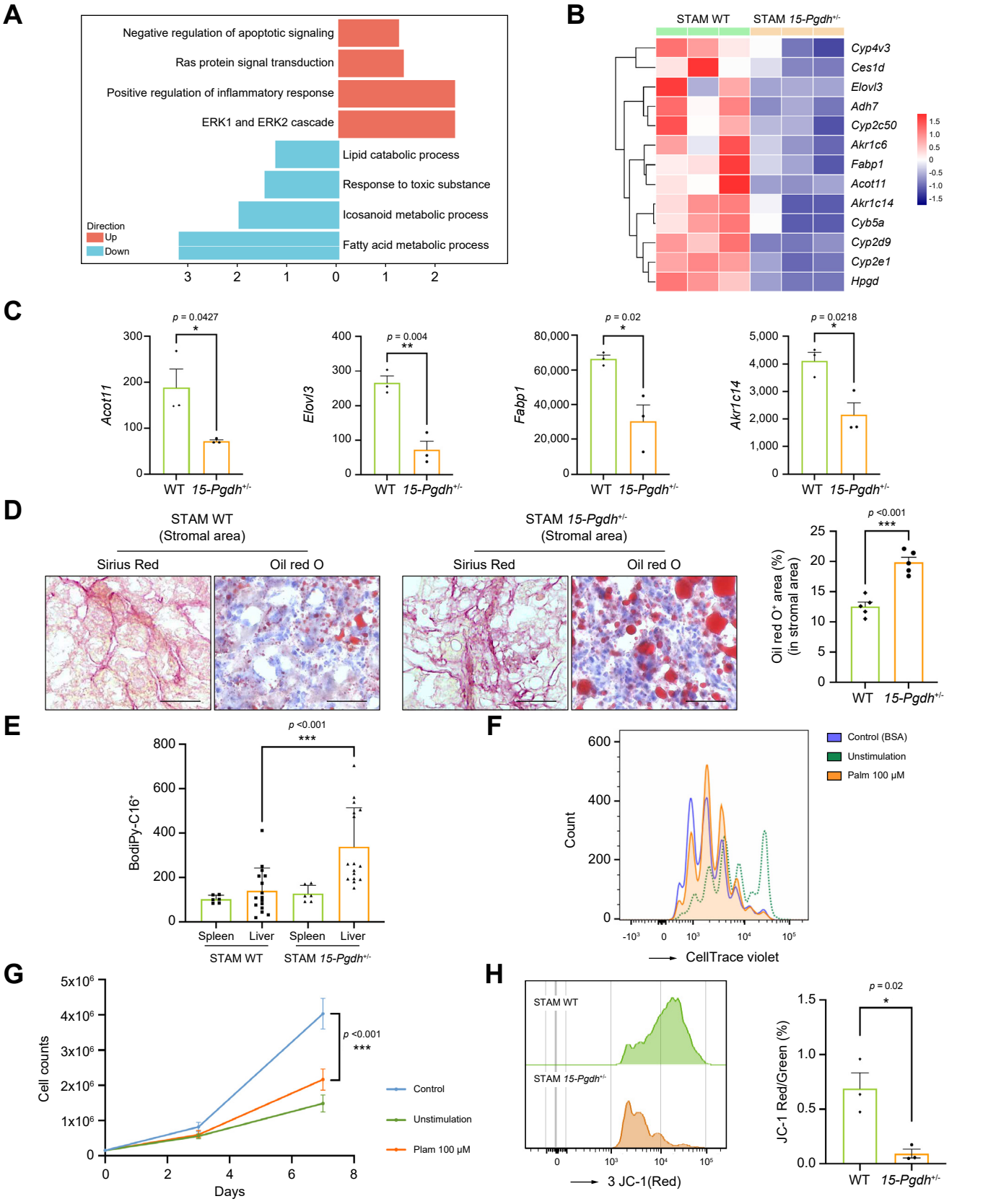

Fig. 4. CD8+ T-cell dysfunction is induced by the accumulation of fatty acids in the background liver of STAM 15-*Pgdh*$^{+/-}$ mice. (A) GO enrichment analysis of up- and downregulated genes involved in fatty acid and lipid metabolism of the background liver of STAM 15-*Pgdh*$^{+/-}$ mice. (B) Heatmap of 13 enriched genes

STAM WT mice (Fig. 3I and K). We further confirmed the increased expression of several key genes related to cell growth and antiapoptotic processes by qRT–PCR (Fig. 3J and L). Supporting the gene expression analysis findings, the number of Ki-67-positive hepatocytes in the background liver was significantly higher in the STAM 15-Pgdh$^{+/-}$ mice than in the STAM WT mice (Fig. 3M). These results suggest that 15-*Pgdh* downregulation could promote hepatocyte proliferation along with increased gene expression related to cell growth and antiapoptotic processes.

The accumulation of fatty acids in the TME caused CD8+ T-cell mitochondrial dysfunction in STAM 15-*Pgdh*$^{+/-}$ mice

Based on the Gene Ontology (GO) enrichment analysis results for downregulated genes identified by RNA sequencing, we found that pathways associated with hepatic fatty acid and lipid metabolism capacity were significantly downregulated in the background livers of STAM 15-*Pgdh*$^{+/-}$ mice (Fig. 4A). The expression of all 13 genes involved in the fatty acid metabolic process was markedly lower in the background liver of STAM 15-*Pgdh*$^{+/-}$ mice than in STAM WT mice (Fig. 4B). We also confirmed the downregulation of the key genes involved in fatty acid elongase activity (*Elovl3*), fatty acid beta-oxidation (*Fabp1*), palmitoyl-CoA hydrolase activity (*Acot11*), and the prostaglandin metabolic process (*Akr1c14*) (Fig. 4C).

Given these findings, we next compared the accumulation of neutral lipids in the liver between STAM WT and 15-Pgdh$^{+/-}$ mice. Oil Red O staining revealed that neutral lipid accumulation was significantly higher in the stromal area of STAM 15-*Pgdh*$^{+/-}$ mice than in that of STAM WT mice, suggesting an excess amount of neutral lipids present in the TME (Fig. 4D). Moreover, we intraperitoneally injected STAM 15-*Pgdh*$^{+/-}$ mice with fluorescently labelled LCFAs (Bodipy-C16), and after 1 h, we analysed CD8+ T cells isolated from background liver tissue by flow cytometry. In STAM WT mice and especially in STAM 15-*Pgdh*$^{+/-}$ mice, CD8+ T cells in liver tissue acquired significantly higher amounts of Bodipy-C16 than control splenic CD8+ T cells (Fig. 4E). Although infiltrating CD8+ T cells can use LCFAs to fuel fatty acid oxidation (FAO) in low-glucose environments, such as in pancreatic ductal adenocarcinoma (PDAC),[24] excessive accumulation of intracellular fatty acids is known to damage cells via lipotoxicity. The levels of Palm and oleic acid were significantly increased compared with those of various other lipid classes in livers with MASH.[25] In particular, Palm has been reported to induce mitochondrial dysfunction in CD8+ T cells.[26] Therefore, we isolated CD8+ T cells from the spleens of WT mice and treated the cells with Palm and Ole. Consequently, we found that both Palm and Ole treatment induced cell cycle arrest and decreased the proliferation of cultured CD8+ T cells in a cell trace assay. However, the effect of Palm was stronger than that of Ole (Fig. 4F and G; Fig. S4A and B). Based on these results, we next considered how the accumulation of fatty acids affects the mitochondrial functions of CD8+ T cells in STAM 15-*Pgdh*$^{+/-}$ mice. We assessed mitochondrial functionality with a JC-1 assay and found a significant reduction in the mitochondrial membrane potential in CD8+ T cells in the background liver of STAM 15-*Pgdh*$^{+/-}$ mice (Fig. 4H). These results indicate that the accumulated lipids have a harmful impact on the mitochondrial functions of CD8+ T cells.

Immune surveillance is inactivated through CD8+ T-cell exhaustion in 15-*Pgdh*$^{+/-}$ mice

Based on these findings, we next investigated whether the reduction in the mitochondrial membrane potential influences CD8+ T-cell impairment. A recent study reported that fatty acid accumulation in the TME in the presence of PDAC reduces CD8+ T-cell infiltration and impairs the mitochondrial function of CD8+ T cells, which leads to the induction of CD8+ T-cell exhaustion.[27,28] Therefore, we hypothesised that 15-*Pgdh* downregulation in the background liver reduces hepatic immune surveillance via the accumulation of fatty acids. To explore our hypothesis, we first compared PD-1 expression in STAM 15-*Pgdh*$^{+/-}$ mice and STAM WT mice. Notably, the expression of PD-1 in CD8+ T cells in the liver of STAM 15-Pgdh$^{+/-}$ mice was significantly increased, whereas the expression in other immune cells (CD4+ T cells, natural killer [NK] cells, and natural killer T [NKT] cells) was not different, suggesting that CD8+ T cells could be affected by 15-*Pgdh* downregulation to reduce immune surveillance (Fig. 5A and B). To further investigate what function of CD8+ T cells was restricted, we examined the ability to secrete effector molecules such as TNF-α and IFN- γ. The results showed that the expression of TNF-α and IFN- γ in CD8+ T cells in the liver was decreased in 15-*Pgdh*$^{+/-}$ STAM mice compared with STAM WT mice (Fig. 5C and D), supporting the hypothesis that CD8+ T-cell exhaustion is induced by 15-*Pgdh* downregulation. Consistent with the findings of the *in vivo* experiments, staining of tissue sections of the background liver revealed that the expression of PD-1 was significantly higher in the 15-PGDH–low patient group (Fig. 5E). The above findings suggest that 15-*Pgdh* downregulation inactivates immune surveillance by promoting the proliferation of exhausted effector T cells, which enhances hepatocyte survival and proliferation and leads to MASH-HCC development.

Discussion

The global incidence of MAFLD/MASH has increased significantly, and recent epidemiological investigations have indicated that in the absence of liver cirrhosis, MAFLD/MASH is the leading cause of HCC.[29] Over the past decade, it has been shown that the expression of COX-2 in acute and chronic liver diseases is abnormally elevated; this inflammatory enzyme has

located upstream of the fatty acid metabolic process in the background liver of STAM 15-*Pgdh*$^{+/-}$ mice. (C) Validation of the upregulation of selected genes involved in the fatty acid metabolic process in the background liver of STAM mice by qRT–PCR. (D) Representative image of Oil Red O staining of the stromal area in STAM WT and 15-*Pgdh*$^{+/-}$ mice. Stromal area was identified using Sirius Red staining. The graph represents the quantification of Oil Red O-positive areas for each group (n = 5/group). Scale bars, 25 μm. (E) Quantification of BODIPY-C16 uptake in infiltrating CD8+ T cells in the background liver of STAM mice after intraperitoneal injection of fluorescently labelled LCFAs (BODIPY-C16). Spleen, control. (F) Cell trace analysis of CD8+ T cells isolated from the spleens of WT mice treated with Palm (n = 2). (G) Cell proliferation of CD8+ T cells isolated from the spleens of WT mice treated with Palm (n = 2). (H) Representative histograms of JC-1 analysis of CD8+ T cells in the background liver of WT and STAM mice. The graph represents the quantification of the ratio of red to green JC-1 fluorescence (percentage) (n = 3/group). *p <0.05, **p <0.01, ***p <0.001 Mann–Whitney *U* test. 15-PGDH, 15-hydroxyprostaglandin dehydrogenase; GO, Gene Ontology; LCFA, long-chain fatty acid; Palm, palmitic acid; STAM, steric animal model; STAM, steric animal model; WT, wild-type.

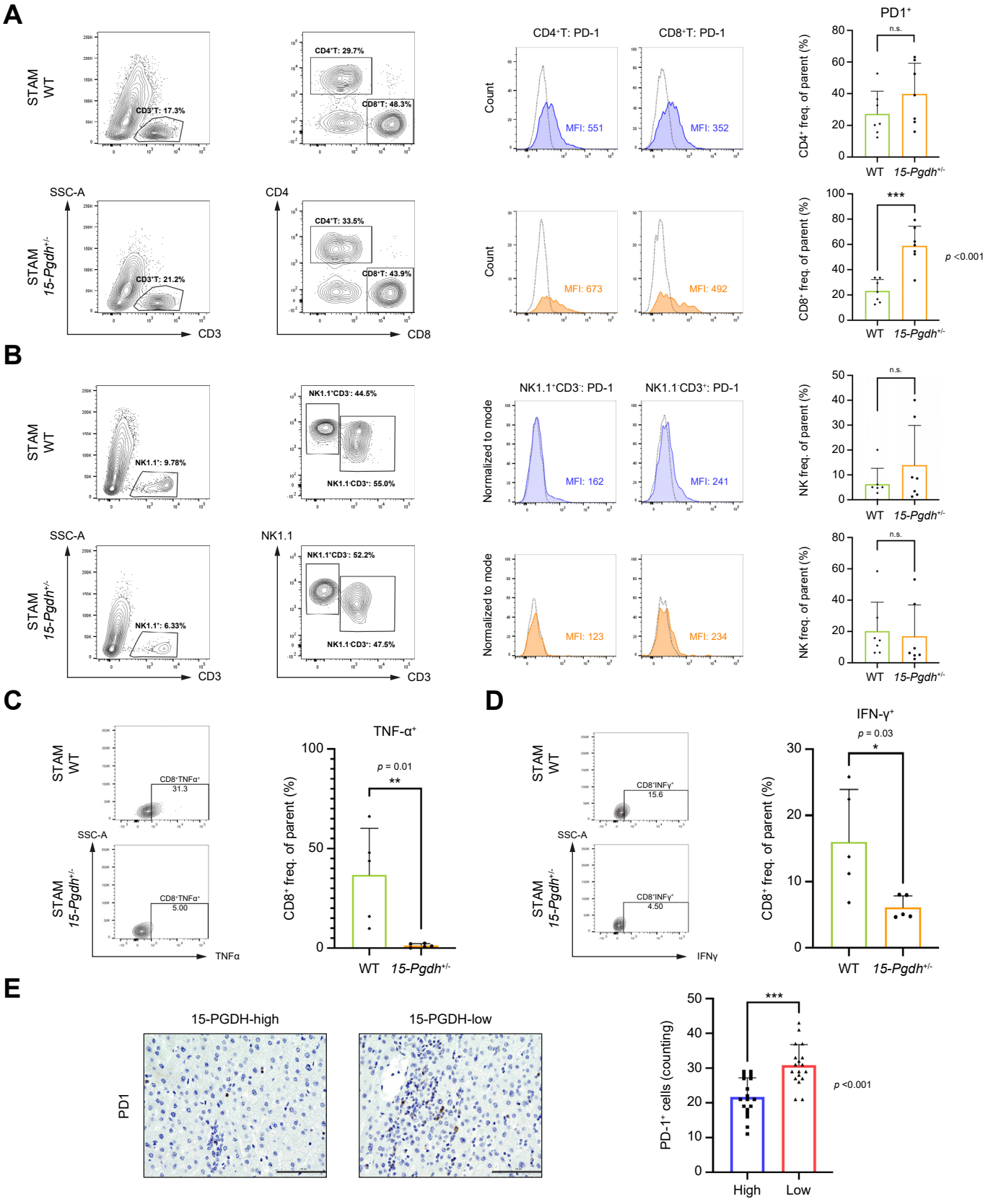
A
STAM WT
CD3+T: 17.3%
CD4+T: 29.7%
CD8+T: 48.3%
CD4+T: PD-1
CD8+T: PD-1
Count
MFI: 551
MFI: 352
PD1+
n.s.
CD4+ freq. of parent (%)
WT
15-Pgdh+/-
STAM 15-Pgdh+/-
SSC-A
CD3
CD4
CD8
CD3+T: 21.2%
CD4+T: 33.5%
CD8+T: 43.9%
MFI: 673
MFI: 492
***
p <0.001
CD8+ freq. of parent (%)
B
STAM WT
NK1.1+: 9.78%
NK1.1+CD3-: 44.5%
NK1.1-CD3+: 55.0%
NK1.1+CD3-: PD-1
NK1.1-CD3+: PD-1
Normalized to mode
MFI: 162
MFI: 241
NK freq. of parent (%)
STAM 15-Pgdh+/-
NK1.1+: 6.33%
NK1.1+CD3-: 52.2%
NK1.1-CD3+: 47.5%
MFI: 123
MFI: 234
C
STAM WT
CD8+TNFα+
31.3
SSC-A
STAM 15-Pgdh+/-
5.00
TNFα
TNF-α+
p = 0.01
**
CD8+ freq. of parent (%)
D
CD8+IFNγ+
15.6
4.50
IFNγ
IFN-γ+
p = 0.03
*
E
15-PGDH-high
15-PGDH-low
PD1
PD-1+ cells (counting)
***
p <0.001
High
Low

been related to cancer progression.[30] In this study, we demonstrated the significance of COX-related signalling; in particular, we focused on the accumulation of endogenous PGE2 and activation of the COX/PGE2 signalling pathway. The accumulation of endogenous PGE2 silences the levels of tumour suppressor genes and DNA repair genes, such as cannabinoid receptor 1 (*CNR1*) and O-6-methylguanine-DNA methyltransferase (*MGMT*), through DNA methylation to promote tumour growth in colon cancer.[31] Our previous studies found that IL-1β secreted by tumour-associated macrophages could downregulate the expression of 15-*PGDH*, an enzyme responsible for degradation of PGE2 in pancreatic ductal cancer. Moreover, *in vivo* experiments performed with a model lacking the 15-*Pgdh* gene demonstrated increased expression of aldehyde dehydrogenase 1 (*Aldh1*), which was found to be negatively correlated with 15-*Pgdh* expression and significantly associated with a poor prognosis in patients with PDAC.[16,32] Moreover, the analysis using a public database described in a previous study[18] revealed that the level of 15-PGDH gradually decreased in an inflammation-dependent manner. Inflammation triggers liver damage, and PGE2 is known to modulate tissue regeneration, stimulating hepatocyte proliferation.[33] This phenomenon represents a characteristic feature of the hepatocarcinogenesis process in HCC known as multistep hepatocarcinogenesis. Hepatocytes that have been damaged by inflammation or other factors undergo regeneration and proliferation, ultimately serving as the origin of HCC.[34] Together with these previous studies, our current findings delineate a molecular mechanism underlying the promotion of PGE2 accumulation by downregulation of 15-*PGDH* expression in the background liver, leading to tumour progression in MASH-HCC.

Another important function of PGE2 is its ability to promote the accumulation of PD-1+ T cells. PGE2 exerts an important function in controlling the equilibrium of Th1, Th2, and Treg cell levels, resulting in the promotion of an immunosuppressive niche and tumour growth in pancreatic carcinoma.[35] To date, blockade of the PD-1 immune checkpoint has been developed as a therapeutic modality in HCC, with anti-PD-1 antibodies, such as nivolumab and pembrolizumab, being introduced to the clinic. The combination of an anti-PDL1 antibody (atezolizumab) with an anti-VEGF antibody (bevacizumab) is a first-line treatment for advanced HCC.[14,36,37] However, less than 30% of patients with HCC respond to immunotherapy.[38] It was recently reported that the levels of aberrant PD-1+CD8+ T cells, which could not perform immune surveillance and exerted tissue-damaging functions in a TNF-dependent manner, were increased by anti-PD-1 treatment in MASH-HCC. This immune environment may contribute to weakening of the efficacy of anti-PD-1 treatment and may even lead to HCC development.[13,39]

Previously, lipotoxicity was shown to be closely associated with MASH severity. Free cholesterol deposited in hepatocyte mitochondria causes hepatocyte apoptosis and necrosis by activating the JNK1 signalling pathway.[40] Moreover, clinical trials focusing on hepatic TG homeostasis have been conducted to normalise lipid metabolism and to reduce the risk of severe MASH.[41] Conversely, recent studies have revealed that lipotoxicity is involved in one aspect of dysfunctional immune surveillance. The accumulation of LCFAs in the TME of patients with advanced pancreatic cancer impairs mitochondrial function and triggers the downregulation of very long-chain acyl-CoA dehydrogenase (VLCAD), which induces the accumulation of LCFAs in intrapancreatic CD8+ T cells.[27] Another report indicated that lipid accumulation increased the expression of CD36, which promotes the uptake of oxidised low-density lipoproteins (OxLDL) in T cells, and this induced lipid peroxidation and downstream activation of p38 kinase, followed by CD8+ T-cell exhaustion.[27] These reports suggest that lipid accumulation in the TME directly contributes to CD8+ T-cell impairment. Supporting this recent evidence, our study revealed that phenotypic changes in lipid metabolism in the background liver influenced the TME, which led to a reduction in the mitochondrial activity of exhausted CD8+ T cells in the MASH-HCC mouse model.

Given that PGE2 accumulation enhances MASH-HCC development by affecting hepatocytes and CD8+ T-cell function, it would be beneficial to consider potential therapeutic interventions. For instance, daily use of aspirin has been found to reduce the risk of adenoma recurrence in patients with a history of colorectal adenoma in randomised controlled trials.[42–45] Recently, inhibition of the COX-2 inhibitor celecoxib was shown to attenuate MAFLD activity by elevating serum adiponectin levels and Adipo-R1 and Adipo-R2 expression levels in the rat liver.[46] Moreover, we investigated the significance of COX2/PGE2 signalling in promoting MASH-HCC development and leading to inactivation of immune surveillance. Together with these previous studies, our present findings suggest that COX-2 inhibitors may represent a potential novel therapy for use in combination with conventional immunotherapy for MASH.

In summary, our study shows that the downregulation of 15-*PGDH* leads to the accumulation of PGE2 in the TME, which induces ROS production in macrophages and the expression of cell

Fig. 5. Immune surveillance was suppressed through CD8+ T-cell exhaustion in STAM 15-Pgdh$^{+/-}$ mice and patients with MASH-HCC. (A) Flow cytometric analysis of PD-1 expression in infiltrating CD4+ and CD8+ T cells in the background liver of STAM mice. Contour plots showing the gating of CD4+ and CD8+ T cells (left). Representative histograms of PD-1 expression in infiltrating CD4+ and CD8+ T cells and quantification of PD-1+ cells in CD4+ or CD8+ T cells (middle, right). (B) Flow cytometric analysis of PD-1 expression in infiltrating NK cells and NKT cells in the background liver of STAM mice. Contour plots show the gating of NK cells and NKT cells (left). Representative histograms of PD-1 expression in infiltrating NK cells and NKT cells and quantification of PD-1+ cells in NK cells and NKT cells (middle, right). (C) Flow cytometric analysis of TNF-α expression in CD8+ T cells in the background liver of STAM mice. Contour plots showing the gating of TNF-α+ immune cells and quantification of TNF-α+ cells in immune cells. (D) Flow cytometric analysis of IFN-γ expression in CD8+ T cells in the background liver of STAM mice. Contour plots showing the gating of TNF-α+CD8+ T cells and quantification of TNF-α+ cells in CD8+ T cells. (E) Representative IHC staining for PD-1 in the background liver of patients with MASH-HCC (n = 10/group). The graph represents the number of PD-1-positive cells per mm3 in four randomly selected areas. Scale bars, 100 μm $^{*}p$ <0.05, $^{**}p$ <0.01, $^{***}p$ <0.001 Mann–Whitney *U* test. ns, not significant; HCC, hepatocellular carcinoma; IHC, immunohistochemistry; MASH, metabolic dysfunction-associated steatohepatitis; NK, natural killer; NKT, natural killer T; PD1, programmed death receptor-1; STAM, steric animal model.

growth-related genes and antiapoptotic genes. In contrast, the downregulation of fatty acid metabolism in hepatocytes during MASH development promotes lipid accumulation in the TME, which leads to reduced mitochondrial activity and an exhausted phenotype in CD8+ T cells. Aberrant hepatocytes that escape immune surveillance exacerbate the development of MASH-HCC. Given these findings, the suppression of PGE2-related inflammation in addition to immune checkpoint blockade may lead to attenuation of MASH and inhibition of subsequent MASH-HCC progression.

Abbreviations

15-PGDH, 15-hydroxyprostaglandin dehydrogenase; Aldh1, aldehyde dehydrogenase 1; ALT, alanine aminotransferase; AST, aspartate aminotransferase; BG, blood glucose; cDNA, complementary DNA; CNR1, cannabinoid receptor 1; COX-2, cyclooxygenase 2; DEGs, differentially expressed genes; FACS, fluorescence-activated cell sorting; FAO, fatty acid oxidation; GO, Gene Ontology; HCC, hepatocellular carcinoma; HFD, high-fat diet; IHC, immunohistochemistry; IL-1β, interleukin-1β; LCFA, long-chain fatty acid; LW/BW, ratio of liver weight to body weight; MAFLD, metabolic dysfunction associated fatty liver disease; MAS, MAFLD activity score; MASH, metabolic dysfunction-associated steatohepatitis; MGMT, O-6-methylguanine-DNA methyltransferase; NAFLD, non-alcoholic fatty liver disease; NASH, non-alcoholic steatohepatitis; NK, natural killer; NKT, natural killer T; Ole, oleic acid; OS, overall survival; OxLDL, oxidised low-density lipoproteins; Palm, palmitoleic acid; PBMCs, peripheral blood mononuclear cells; PD-1, programmed death receptor; PDAC, pancreatic ductal adenocarcinoma; PGE2, prostaglandin E2; RFS, recurrence-free survival; ROS, reactive oxygen species; RT, reverse transcription; SEs, standard errors; SNVs, single-nucleotide variants; STAM, steric animal model; TG, triglycerides; TME, tumour microenvironment; VLCAD, very long chain acyl-CoA dehydrogenase; WES, whole-exome sequencing; WT, wild-type.

Financial support

This work was supported by the FOREST program of the Japan Science and Technology Agency (JST, grant no. JPMJFR200H to T.I.), AMED (grant no. 23ama221421 to T.I.), the Japan Society for the Promotion of Science (JSPS, KAKENHI grant nos. 20K09038, 21KK0153 and 23H02772 to T.I.; 23K08051 to T.Y.; and 23H02998 to T.S.), the Suzuken Memorial Foundation, the Chugai Foundation for Innovative Drug Discovery Science, and the Shinnihon Foundation of Advanced Medical Treatment Research.

Conflicts of interest

The authors declare that they have no competing interests to disclose.

Please refer to the accompanying ICMJE disclosure forms for further details.

Authors' contributions

Conception and design: TY, TI. Data acquisition: XH, NY, AY, TU. Data analysis and interpretation (e.g., RNA sequencing and computational analysis): XH, TY, NY, AY, TU, YN, KY, TI. Manuscript writing, review, and/or revision: XH, TY, KY, TI. Administrative, technical, or material support: TS, KA, TU, AN, LB, LF, FW, JZ, YT, HW. Study supervision: KI, TF, HN, KT, YM, HB, TI.

Data availability statement

The whole-exome sequencing data were deposited in the DDBJ database under accession number DRA016752. The RNA-sequencing data were deposited in the DDBJ database under accession number DRA016740. All datasets generated during the current study are available from the corresponding authors upon request.

Acknowledgments

The authors thank Y. Takahashi (Department of Anatomy and Neurobiology, Graduate School of Medical Sciences, Kumamoto University) for assisting with the staining of sections.

Supplementary data

Supplementary data to this article can be found online at https://doi.org/10.1016/j.jhepr.2023.100892.

References

[1] Llovet JM, Kelley RK, Villanueva A, Singal AG, Pikarsky E, Roayaie S, et al. Hepatocellular carcinoma. Nat Rev Dis Primers 2021;7:1–28.
[2] Rinella ME, Lazarus JV, Ratziu Vlad, Francque SM, Sanyal AJ, Kanwal F, et al. A multi-society Delphi consensus statement on new fatty liver disease nomenclature. JHEP Rep 2023:S0168-8278(23)00418-X. https://doi.org/10.1016/j.jhep.2023.06.003.
[3] Mantovani A, Allavena P, Sica A, Balkwill F. Cancer-related inflammation. Nature 2008;454:436–444.
[4] Eslam M, Valenti L, Romeo S. Genetics and epigenetics of NAFLD and NASH: clinical impact. J Hepatol 2018;68:268–279.
[5] Diehl AM, Day C. Cause, pathogenesis, and treatment of nonalcoholic steatohepatitis. N Engl J Med 2017;377:2063–2072.
[6] Villanueva A. Hepatocellular carcinoma. N Engl J Med 2019;380:1450–1462.
[7] Smith WL, Urade Y, Jakobsson P-J. Enzymes of the cyclooxygenase pathways of prostanoid biosynthesis. Chem Rev 2011;111:5821–5865.
[8] Wang D, DuBois RN. Role of prostanoids in gastrointestinal cancer. J Clin Invest 2018;128:2732–2742.
[9] Myung S-J, Rerko RM, Yan M, Platzer P, Guda K, Dotson A, et al. 15-Hydroxyprostaglandin dehydrogenase is an *in vivo* suppressor of colon tumourigenesis. Proc Natl Acad Sci U S A 2006;103:12098–12102.
[10] Prima V, Kaliberova LN, Kaliberov S, Curiel DT, Kusmartsev S. COX2/mPGES1/PGE2pathway regulates PD-L1 expression in tumour-associated macrophages and myeloid-derived suppressor cells. Proc Natl Acad Sci U S A 2017;114:1117–1122.
[11] Kim H-B, Kim M, Park Y-S, Park I, Kim T, Yang S-Y, et al. Prostaglandin E2 activates YAP and a positive-signaling loop to promote colon regeneration after colitis but also carcinogenesis in mice. Gastroenterology 2017;152:616–630.
[12] Pinter M, Pinato DJ, Ramadori P, Heikenwalder M. NASH and hepatocellular carcinoma: immunology and immunotherapy. Clin Cancer Res 2023 Feb 1;29(3):513–520. https://doi.org/10.1158/1078-0432.CCR-21-1258.
[13] Pfister D, Núñez NG, Pinyol R, Govaere O, Pinter M, Szydlowska M, et al. NASH limits anti-tumour surveillance in immunotherapy-treated HCC. Nature 2021;592:450–456.
[14] Yau T, Kang Y-K, Kim T-Y, El-Khoueiry AB, Santoro A, Sangro B, et al. Efficacy and safety of nivolumab plus ipilimumab in patients with advanced hepatocellular carcinoma previously treated with sorafenib. JAMA Oncol 2020;6:e204564.
[15] Kleiner DE, Brunt EM, Van Natta M, Behling C, Contos MJ, Cummings OW, et al. Design and validation of a histological scoring system for nonalcoholic fatty liver disease. Hepatology 2005;41:1313–1321.
[16] Arima K, Ohmuraya M, Miyake K, Koiwa M, Uchihara T, Izumi D, et al. Inhibition of 15-PGDH causes Kras-driven tumour expansion through prostaglandin E2-ALDH1 signaling in the pancreas. Oncogene 2018;38:1211–1224.
[17] Blokzijl F, Janssen R, van Boxtel R, Cuppen E. MutationalPatterns: comprehensive genome-wide analysis of mutational processes. Genome Med 2018;10:33.
[18] Boldanova T, Suslov A, Heim MH, Necsulea A. Transcriptional response to hepatitis C virus infection and interferon-alpha treatment in the human liver. EMBO Mol Med 2017;9:816–834.
[19] Bu L, Yonemura A, Yasuda-Yoshihara N, Uchihara T, Ismagulov G, Takasugi S, et al. Tumour microenvironmental 15-PGDH depletion promotes fibrotic tumour formation and angiogenesis in pancreatic cancer. Cancer Sci 2022;113:3579–3592.
[20] Bian X, Chen H, Yang P, Li Y, Zhang F, Zhang J, et al. Nur77 suppresses hepatocellular carcinoma via switching glucose metabolism toward gluconeogenesis through attenuating phosphoenolpyruvate carboxykinase sumoylation. Nat Comm 2017;8:14420.
[21] Kim SY, Jeong J-M, Kim SJ, Seo W, Kim M-H, Choi W-M, et al. Pro-inflammatory hepatic macrophages generate ROS through NADPH oxidase 2

via endocytosis of monomeric TLR4–MD2 complex. Nat Comm 2017;8:2247.
[22] Formentini L, Santacatterina F, Núñez de Arenas C, Stamatakis K, López-Martínez D, Logan A, et al. Mitochondrial ROS production protects the intestine from inflammation through functional M2 macrophage polarization. Cell Rep 2017;19:1202–1213.
[23] Manders F, Brandsma AM, de Kanter J, Verheul M, Oka R, van Roosmalen MJ, et al. MutationalPatterns: the one stop shop for the analysis of mutational processes. BMC Genomics 2022;23:134.
[24] O'Sullivan D, van der Windt GJW, Huang SC-C, Curtis JD, Chang C-H, Buck MD, et al. Memory CD8+ T cells use cell-intrinsic lipolysis to support the metabolic programming necessary for development. Immunity 2014;41:75–88.
[25] Puri P, Wiest MM, Cheung O, Mirshahi F, Sargeant C, Min H-K, et al. The plasma lipidomic signature of nonalcoholic steatohepatitis. Hepatology 2009;50:1827–1838.
[26] de Pablo MA, Susin SA, Jacotot E, Larochette N, Costantini P, Ravagnan L, et al. Palmitate induces apoptosis via a direct effect on mitochondria. Apoptosis 1999;4:81–87.
[27] Manzo T, Prentice BM, Anderson KG, Raman A, Schalck A, Codreanu GS, et al. Accumulation of long-chain fatty acids in the tumour microenvironment drives dysfunction in intrapancreatic CD8+ T cells. J Exp Med 2020;217:e20191920.
[28] Xu S, Chaudhary O, Rodríguez-Morales P, Sun X, Chen D, Zappasodi R, et al. Uptake of oxidized lipids by the scavenger receptor CD36 promotes lipid peroxidation and dysfunction in CD8+ T cells in tumours. Immunity 2021;54:1561–1577.e7.
[29] Ioannou GN. Epidemiology and risk-stratification of NAFLD-associated HCC. J Hepatol 2021;75:1476–1484.
[30] Hashemi Goradel N, Najafi M, Salehi E, Farhood B, Mortezaee K. Cyclooxygenase-2 in cancer: a review. J Cell Physiol 2018;234:5683–5699.
[31] Xia D, Wang D, Kim S-H, Katoh H, DuBois RN. Prostaglandin E2 promotes intestinal tumour growth via DNA methylation. Nat Med 2012;18:224–226.
[32] Arima K, Komohara Y, Bu L, Tsukamoto M, Itoyama R, Miyake K, et al. Downregulation of 15-hydroxyprostaglandin dehydrogenase by interleukin-1β from activated macrophages leads to poor prognosis in pancreatic cancer. Cancer Sci 2018;109:462–470.
[33] Cheng H, Huang H, Guo Z, Chang Y, Li Z. Role of prostaglandin E2 in tissue repair and regeneration. Theranostics 2021;11:8836–8854.
[34] Holczbauer A, Wangensteen KJ, Shin S. Cellular origins of regenerating liver and hepatocellular carcinoma. JHEP Rep 2022;4. 100416–6.
[35] Finetti F, Travelli C, Ercoli J, Colombo G, Buoso E, Trabalzini L. Prostaglandin E2 and cancer: insight into tumour progression and immunity. Biology 2020;9:434.
[36] Finn RS, Qin S, Ikeda M, Galle PR, Ducreux M, Kim T-Y, et al. Atezolizumab plus bevacizumab in unresectable hepatocellular carcinoma. N Engl J Med 2020;382:1894–1905.
[37] Finn RS, Ikeda M, Zhu AX, Sung MW, Baron AD, Kudo M, et al. Phase Ib study of lenvatinib plus pembrolizumab in patients with unresectable hepatocellular carcinoma. J Clin Oncol 2020;38:2960–2970.
[38] Yau T, Park J-W, Finn RS, Cheng A-L, Mathurin P, Edeline J, et al. Nivolumab versus sorafenib in advanced hepatocellular carcinoma (CheckMate 459): a randomised, multicentre, open-label, phase 3 trial. Lancet Oncol 2022;23:77–90.
[39] Haber PK, Puigvehí M, Castet F, Lourdusamy V, Montal R, Tabrizian P, et al. Evidence-based management of hepatocellular carcinoma: systematic review and meta-analysis of randomized controlled trials (2002–2020). Gastroenterology 2021;161:879–898.
[40] Gan LT, Van Rooyen DM, Koina ME, McCuskey RS, Teoh NC, Farrell GC. Hepatocyte free cholesterol lipotoxicity results from JNK1-mediated mitochondrial injury and is HMGB1 and TLR4-dependent. J Hepatol 2014;61:1376–1384.
[41] Neuschwander-Tetri BA, Loomba R, Sanyal AJ, Lavine JE, Van Natta ML, Abdelmalek MF, et al. Farnesoid X nuclear receptor ligand obeticholic acid for non-cirrhotic, non-alcoholic steatohepatitis (FLINT): a multicentre, randomised, placebo-controlled trial. Lancet 2015;385:956–965.
[42] Logan RFA, Grainge MJ, Shepherd VC, Armitage NC, Muir KR. Aspirin and folic acid for the prevention of recurrent colorectal adenomas. Gastroenterology 2008;134:29–38.
[43] Baron JA, Cole BF, Sandler RS, Haile RW, Ahnen D, Bresalier R, et al. A randomized trial of aspirin to prevent colorectal adenomas. N Engl J Med 2003;348:891–899.
[44] Benamouzig R, Deyra J, Martin A, Girard B, Jullian E, Piednoir B, et al. Daily soluble aspirin and prevention of colorectal adenoma recurrence: one-year results of the APACC trial. Gastroenterology 2003;125:328–336.
[45] Sandler RS, Halabi S, Baron JA, Budinger S, Paskett E, Keresztes R, et al. A randomized trial of aspirin to prevent colorectal adenomas in patients with previous colorectal cancer. N Engl J Med 2003;348:883–890.
[46] Zhu G, Chen L, Liu S, She L, Ding Y, Yang C, et al. Celecoxib-mediated attenuation of non-alcoholic steatohepatitis is potentially relevant to redistributing the expression of adiponectin receptors in rats. Heliyon 2022;8:e09872.